PHYSICAL REVIEW A **96**, 042306 (2017)

High-fidelity Rydberg quantum gate via a two-atom dark state

David Petrosyan,[1,2] Felix Motzoi,[1] Mark Saffman,[3] and Klaus Mølmer[1]
[1]*Department of Physics and Astronomy, Aarhus University, DK-8000 Aarhus C, Denmark*
[2]*Institute of Electronic Structure and Laser, FORTH, GR-71110 Heraklion, Crete, Greece*
[3]*Department of Physics, University of Wisconsin—Madison, Madison, Wisconsin 53706, USA*
(Received 7 August 2017; published 9 October 2017)

We propose a two-qubit gate for neutral atoms in which one of the logical state components adiabatically follows a two-atom dark state formed by the laser coupling to a Rydberg state and a strong resonant dipole-dipole exchange interaction between two Rydberg excited atoms. Our gate exhibits optimal scaling of the intrinsic error probability $E \propto (B\tau)^{-1}$ with the interatomic interaction strength B and the Rydberg state lifetime τ. Moreover, the gate is resilient to variations in the interaction strength, and even for finite probability of double Rydberg excitation the gate does not excite atomic motion and experiences no decoherence due to internal-translational entanglement.

DOI: 10.1103/PhysRevA.96.042306

I. INTRODUCTION

Strong long-range interactions between atoms excited to the Rydberg states with large principal quantum numbers n make them attractive systems for the studies of few- and many-body physics and for quantum information applications [1]. Different schemes of interatomic interactions are employed in this research, ranging from the blockade of multiple Rydberg excitations of nearby atoms by resonant laser fields [1–3], and the antiblockade nonresonant (facilitated) laser excitation [4–8], to the Rydberg dressing of the ground-state atoms by very far-off-resonant lasers [9–15].

The Rydberg state interatomic interactions hold unique potential for the implementation of quantum gates with spatially separated neutral atoms. In the seminal proposal of Jaksch *et al.* [16], each qubit is encoded in a pair of (meta)stable states $|0\rangle$ and $|1\rangle$ of an atom, and two-qubit gate operations are performed by selectively exciting a pair of atoms from specific qubit states, e.g., $|1\rangle$, to the interacting Rydberg states. In the regime of a weak dispersive interaction, the pair of Rydberg excited atoms acquires an interaction-induced phase shift, which is then transferred to the corresponding two-qubit state $|11\rangle$ by coherently deexciting the atoms. In the alternative regime of strong interaction, if one (control) atom is resonantly excited to the Rydberg state, the interaction-induced level shift suppresses Rydberg excitation of the second (target) atom within a distance of several micrometers. Ideally, this blockade effect [1–3] does not depend on the precise value of the interaction strength, as long as it is sufficiently strong to completely preclude multiple Rydberg excitations. Since at most one atom is excited to the Rydberg state at a time, the interaction potential does not induce interatomic forces, which would otherwise entangle the internal (qubit) and external (motional) degrees of freedom of the atoms. The Rydberg blockade gate has therefore been the preferred choice for quantum logic gate operations [16–20].

The performance of the Rydberg blockade gate has been extensively analyzed [21–24], taking into account various experimental imperfections and fundamental limitations of the scheme. Assuming that technical errors due to, e.g., laser phase and amplitude fluctuations and finite temperature atomic motion and Doppler shifts can be eliminated, and that leakage errors to the unwanted Rydberg states can be suppressed by using, e.g., shaped laser pulses [24], the remaining limitations of the standard blockade gate stem from the finite lifetime $\tau = 1/\Gamma \propto n^3$ of the Rydberg states, duration $T \simeq 2\pi/\Omega$ of the gate performed by excitation lasers with Rabi frequency $\Omega \gg \Gamma$, and finite Rydberg-Rydberg interaction strength $B \gg \Omega$. Two types of intrinsic errors have been identified: the error $E_{\rm decay} \simeq 2\pi\Gamma/\Omega$ due to the decay of the Rydberg states during the gate time T, and the rotation error $E_{\rm rot} \simeq \Omega^2/2B^2$ due to imperfect blockade of double Rydberg excitation. Minimizing the total error $E = E_{\rm decay} + E_{\rm rot}$ with respect to Ω leads then to $E \propto (\Gamma/B)^{2/3}$ scaling of the intrinsic error [23]. The resulting estimates for the gate error probability ($E \sim 10^{-3}$) are above the required threshold values for fault tolerant quantum computation. We recall that scaling the quantum hardware in order to tackle problems for which quantum computers may outperform their classical counterparts entails low threshold values of the gate error probabilities: $E \simeq 2 \times 10^{-5}$ for use of the [7,1,3] Steane and [9,1,3] Bacon-Shor error correction codes [25,26], and $E \simeq 4 \times 10^{-4}$ for use of the Knill C4/C6 code [27].

Here we propose and analyze an improved mechanism for implementing entangling two-atom Rydberg gates. Our gate is similar to the Rydberg blockade gate, but with an important difference. As in the standard blockade gate, we excite the control and target atoms from the qubit states $|1_{\rm c,t}\rangle$ to the Rydberg states $|r_{\rm c,t}\rangle$. But instead of relying on the interaction-induced level shift of a pair of Rydberg states, we employ adiabatic following of the two-atom dark state that exists when the atoms in state $|r_{\rm c}r_{\rm t}\rangle$ can undergo strong resonant dipole-dipole exchange interaction with another Rydberg-product state $|a_{\rm c}b_{\rm t}\rangle$. By using a smooth 2π laser pulse to resonantly drive the target atom, we ensure that all of the residual Rydberg state population adiabatically returns back to the qubit state $|1_{\rm t}\rangle$, eliminating thereby the rotation error $E_{\rm rot}$. The minimal intrinsic error then scales as $E \propto (\Gamma/B)$, with $\Omega/B \ll 1$, and it can reach values as small as $E \sim 10^{-5}$ for the Rydberg states with $n \gtrsim 100$.

In the following sections, we present the quantitative description of our scheme, estimates of the smallest achievable intrinsic error probability of the gate, and the results of numerical simulations. In Appendix A we outline the essentials of the resonant Förster process for properly tuned Rydberg

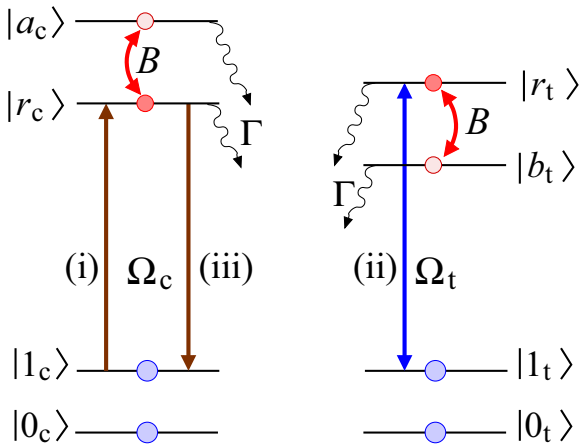

FIG. 1. Level scheme of two atoms leading to a Rydberg phase gate by three focused laser pulses. States $|0_{c,t}\rangle$ and $|1_{c,t}\rangle$ are long-lived qubit basis states of the control (c) and target (t) atoms, and states $|r_{c,t}\rangle$ and $|a_c\rangle$, $|b_t\rangle$ are Rydberg states with decay rate Γ. In steps i and iii the control atom in state $|1_c\rangle$ is resonantly excited and deexcited to state $|r_c\rangle$ by a laser with Rabi frequency Ω_c and pulse area π, and in step ii the target atom in state $|1_t\rangle$ is resonantly coupled to state $|r_t\rangle$ by another laser with Rabi frequency Ω_t and pulse area 2π. Atoms excited to Rydberg states $|r_c\rangle$ and $|r_t\rangle$ strongly interact with each other, $B \gg \Omega_t$, via resonant dipole-dipole exchange process $|r_c r_t\rangle \leftrightarrow |a_c b_t\rangle$ which leads to suppression of excitation of the target atom in step ii if the control was initially in state $|1_c\rangle$. We assume that atoms in state $|0\rangle$ are decoupled from the laser fields.

states of atoms to realize our two-atom dark state, while detailed description of the two-atom systems is given in Appendix B. In Appendix C we show that using adiabatic pulses for the conventional blockade gate also eliminates rotation errors and improves its performance. In contrast to the conventional gates, however, in our scheme the uncertainty in the interaction strength does not lead to phase errors, and despite the nonvanishing probability of double Rydberg excitation there is no mechanical force between the atoms, which would otherwise hinder the operation of both the interaction and blockade gates with the Rydberg excited atoms [28–30].

II. THE DARK STATE ADIABATIC GATE

In Fig. 1 we show the relevant energy levels of two atoms for realizing the Rydberg quantum gate. The qubit basis states are represented by a pair of long-lived hyperfine ground-state sublevels $|0\rangle$ and $|1\rangle$ which can be manipulated by a microwave (MW) field or an optical Raman transition [31,32]. States $|1_{c,t}\rangle$ of the control and target atoms can be coherently coupled to the Rydberg states $|r_{c,t}\rangle$, respectively, by focused laser fields. The atoms excited to the Rydberg states $|r_c\rangle$ and $|r_t\rangle$ undergo a resonant dipole-dipole exchange process $|r_c r_t\rangle \leftrightarrow |a_c b_t\rangle$ with the energy-degenerate pair of Rydberg states $|a_c\rangle$ and $|b_t\rangle$. The dipole-dipole interaction strength $B = C_3/x^3$ depends on the interatomic distance x and the coefficient $C_3 \propto \wp_{a_c r_c} \wp_{r_t b_t}$ is determined by the product of the dipole matrix elements $\wp \propto n^2$ of the transitions $|r_c\rangle \to |a_c\rangle$ and $|r_t\rangle \to |b_t\rangle$ between the Rydberg states with large principal quantum number $n \sim 100$ (see Appendix A).

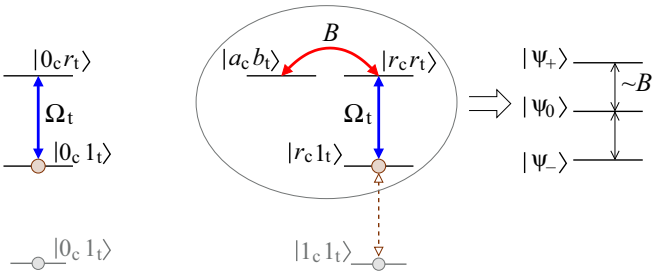

FIG. 2. Evolution of the two-atom system during step ii of the Rydberg-exchange phase gate. Left: The initial two-qubit state $|0_c 1_t\rangle$ remains unchanged after step i, and during step ii the target atom undergoes a 2π Rabi cycle via state $|0_c r_t\rangle$. Middle: The initial two-qubit state $|1_c 1_t\rangle$ is converted to $|r_c 1_t\rangle$ after step i, and during step ii the resonant dipole-dipole exchange interaction $|r_c r_t\rangle \leftrightarrow |a_c b_t\rangle$ with strength $B \gg \Omega_t$ leads to the formation of a two-atom dark state $|\psi_0\rangle$ and two bright states $|\psi_\pm\rangle$ shifted by $\pm B$ (right). In our protocol, state $|r_c 1_t\rangle$ adiabatically follows the dark state $|\psi_0\rangle$ as the target pulse Ω_t is turned on and off.

Our gate procedure is carried out in three steps i–iii, similar to those of the Rydberg blockade protocol [16]. In steps i and iii, resonant pulses of area $\theta_c \equiv \int \Omega_c dt = \pi$ are applied to the control atom. For the initial state $|1_c\rangle$, this amounts to the transitions $|1_c\rangle \to i|r_c\rangle$ in step i and $i|r_c\rangle \to -|1_c\rangle$ in step iii. State $|0_c\rangle$ is assumed completely decoupled from the lasers, due to transition selection rules or large transition frequency mismatch augmented by properly shaped laser pulses. In step ii, a resonant pulse of area $\theta_t \equiv \int \Omega_t dt = 2\pi$ is applied to the target atom resulting in the full Rabi cycle $|1_t\rangle \to i|r_t\rangle \to -|1_t\rangle$ if the control atom is in state $|0_c\rangle$. If, however, in step i the control atom was excited from state $|1_c\rangle$ to the Rydberg state $|r_c\rangle$, the strong dipole-dipole exchange interaction B would result in the two-atom dark state suppressing the target atom Rydberg excitation by the smooth pulse Ω_t, as detailed below. Here again we assume that the target atom in state $|0_t\rangle$ remains decoupled from the laser. Steps i–iii would ideally result in a sign change (π phase shift) of the two-qubit states $|01\rangle, |10\rangle, |11\rangle$ relative to $|00\rangle$. In combination with a Hadamard gate ($\pi/2$ rotation on the $|0_t\rangle \leftrightarrow |1_t\rangle$ transition) applied to the target qubit before and after the phase gate, this leads to the universal CNOT gate between the control and target qubits [33,34].

Hence, out of four possible initial two-qubit states $|00\rangle, |01\rangle, |10\rangle, |11\rangle$, only the last one will probe the Rydberg-Rydberg interaction during step ii. We shall therefore consider in more detail the dynamics of the initial two-atom state $|1_c 1_t\rangle$, which becomes $|r_c 1_t\rangle$ after step i (see Fig. 2). A pulsed laser field with Rabi frequency Ω_t (and area $\theta_t = 2\pi$) acts resonantly on the transition $|1_t\rangle \to |r_t\rangle$ of the target atom, while the two-atom state $|r_c r_t\rangle$ is resonantly coupled to state $|a_c b_t\rangle$ with strength B. The Hamiltonian for the effective three-state system is then

$$H_3/\hbar = \tfrac{1}{2}\Omega_t |r_c r_t\rangle\langle r_c 1_t| + B|a_c b_t\rangle\langle r_c r_t| + \text{H.c.} \qquad (1)$$

This Hamiltonian has three eigenstates:

$$|\psi_0\rangle = \big(B|r_c 1_t\rangle - \tfrac{1}{2}\Omega_t |a_c b_t\rangle\big)/\nu, \qquad (2a)$$

$$|\psi_\pm\rangle = \big(\tfrac{1}{2}\Omega_t |r_c 1_t\rangle \mp \nu |r_c r_t\rangle + B|a_c b_t\rangle\big)/\sqrt{2}\nu, \qquad (2b)$$

with $\nu^2 \equiv B^2 + \frac{1}{4}\Omega_t^2$, and the corresponding eigenvalues are $\lambda_0 = 0$ and $\lambda_\pm = \pm\nu$. The zero-energy eigenstate $|\psi_0\rangle$ does not contain the intermediate state $|r_c r_t\rangle$, and it is customary to call it a dark state [35]. The energy shifted eigenstates $|\psi_\pm\rangle$, with $\lambda_\pm \simeq \pm B$ ($B > \Omega_t$), are similarly called bright states.

Before the laser pulse is switched on, $\Omega_t(0) = 0$, the two-atom state $|r_c 1_t\rangle$ coincides with the dark state $|\psi_0\rangle$. During the application of the pulse $\Omega_t(t)$, if it is sufficiently smooth, $|\partial_t \Omega_t| \ll B|\lambda_\pm - \lambda_0| \simeq B^2$, the system adiabatically follows the dark state, and the bright states $|\psi_\pm\rangle$ are never populated [34,35]. For a smooth envelope $\Omega_t(t)$, the pulse bandwidth is mainly determined by its duration $T_t \approx 2\pi/\Omega_{t0}$, where Ω_{t0} is the mean amplitude. Then the adiabatic following condition $|\partial_t \Omega_t| \approx \Omega_{t0}/T_t \ll B^2$ reduces to $\Omega_{t0} \ll B$, while we assume throughout that $\Omega_{t0} \gg \Gamma$.

The dark state $|\psi_0(t)\rangle$ involves instantaneous population $P_{Ry}(t) = \frac{\Omega_t^2(t)}{4B^2+\Omega_t^2(t)}$ of the two-atom Rydberg state $|a_c b_t\rangle$. During the gate time T_t, this population contributes $\Gamma \int_0^{T_t} P_{Ry}(t)dt \approx \pi\Gamma\Omega_{t0}/4B^2$ to the decay error. At the end of the pulse, $\Omega_t(t \to T_t) \to 0$, and the dark state adiabatically returns to state $|r_c 1_t\rangle$. This state has not accumulated any phase (see below), since the adiabatically connected eigenstate $|\psi_0\rangle$ has energy $\lambda_0 = 0$ for all times $t \in [0, T_t]$. Moreover, even though the double Rydberg excitation state $|a_c b_t\rangle$ has finite occupation probability P_{Ry} while the $\Omega_t(t)$ pulse is on, there is no mechanical force between the atoms, since the gradient of energy of the two-atom eigenstate $|\psi_0\rangle$ identically vanishes, $\partial_x \lambda_0 = 0 \; \forall \; t \in [0, T_t]$. Note that if the adiabatic condition is not satisfied, after the pulse the target atom will have a residual Rydberg population $P_{Ry} \simeq \frac{\Omega_t^2}{4B^2}$ representing a rotation error.

III. RESULTS AND DISCUSSION

The Rydberg states of atoms decay with rate Γ. In order to minimize the error $E_{decay} \simeq \Gamma T_c$ due to decay of the control atom, we thus need to accomplish steps i and iii in shortest possible times using strong pulses of mean amplitude Ω_{c0} and duration $T_c = \pi/\Omega_{c0}$. Similarly, to minimize the error $E_{decay} \simeq \Gamma T_t$ due to the Rydberg state decay of either the control atom or the target atom during step ii, $T_t \approx 2\pi/\Omega_{t0}$, we should take the mean Rabi frequency Ω_{t0} as large as possible, but it should still be smaller than the interaction B, to satisfy the adiabatic following condition detailed above. It then follows that, for the gate performed with a smooth (adiabatic) pulse Ω_t, during step ii the intrinsic error probability averaged over all the possible two-qubit inputs is

$$E \simeq \frac{\pi\Gamma}{4}\left[\frac{5}{\Omega_{t0}} + \frac{\Omega_{t0}}{4B^2}\right]. \tag{3}$$

If we minimize E with respect to Ω_{t0}, we find $E = \frac{\sqrt{5}\pi\Gamma}{4B}$ for $\Omega_{t0} = 2\sqrt{5}B$, which, however, violates the adiabatic criterion. Furthermore, such a large Rabi frequency $\Omega_{t0} \gtrsim B$ is difficult to achieve experimentally for high-lying Rydberg states. Instead, we can choose $\Omega_{t0} = \alpha B$ with $\alpha \ll 1$, obtaining $E \simeq \frac{5\pi\Gamma}{4\Omega_{t0}}$, or $E \simeq \eta\frac{\Gamma}{B}$ with $\eta \simeq \frac{5\pi}{4\alpha}$.

We can estimate the minimum attainable error as follows. In a cryogenic environment with no blackbody radiation, the radiative lifetime of the $ns, np, \ldots$ Rydberg states of the alkali atoms is given by $\tau = 1/\Gamma \approx 10^{-9} n^3$ s [36–38]. The strongest interaction is achieved with the dipole-dipole potential $B \simeq \frac{1}{\hbar}\frac{\wp^2}{4\pi\epsilon_0 x^3}$, where $\wp \sim a_0 e n^2$ is the dipole moment of the atom in the Rydberg state. At the interatomic distance of $x = 3$–5 μm, we then have $B \simeq 100 n^4$ rad/s. To avoid population leakage to other Rydberg states, this interaction strength should be smaller than the level separation between neighboring n states, $\delta\omega_F \sim 2\mathrm{Ry} n^{-3} > B$ (see Appendix A). This then leads to the condition $n \lesssim 100$, which also follows from the requirement that the Rydberg electron clouds (of size $\sim a_0 n^2$) of neighboring atoms do not overlap. We thus obtain $B\tau \approx 10^{-7} n^7 \sim 10^7$ for $n \sim 100$. Choosing $\alpha = \Omega_t/B \simeq 0.1$ ($\eta \simeq 40$), the minimal error probability is $E \simeq \eta\frac{\Gamma}{B} \lesssim 10^{-5}$.

We note that general arguments [39] put a lower limit $E \simeq \frac{2\Gamma}{B}$ on the gate error due to decay of the interacting excited states, which is an order of magnitude smaller than in our case. This is due to our requirement of adiabatic, i.e., slow, evolution of the system to avoid population leakage to undesired states. To speed up the gate and reduce the accumulated decay probability of the Rydberg states, one may resort to recently developed "shortcut to adiabaticity" schemes [40]. In particular, using the so-called derivative removal by adiabatic gate pulses [24,41] may accelerate the gate by operating in the regime of $\Omega_{t0} \sim B$, provided the necessary laser intensities can be achieved.

As we discuss in Appendices A and B, the Rydberg product states $|r_c r_t\rangle$ and $|a_c b_t\rangle$ might experience nonresonant dipole-dipole couplings to other Rydberg pair states. While population leakage to these states is reduced in the adiabatic regime, dispersive coupling with these states will result in second-order (van der Waals) energy shifts β_{rr} and β_{ab} of states $|r_c r_t\rangle$ and $|a_c b_t\rangle$. The two-atom dark state $|\psi_0\rangle$ does not involve the population of the intermediate state $|r_c r_t\rangle$ and is insensitive to its energy shifts β_{rr}. But the energy shift β_{ab} of state $|a_c b_t\rangle$ perturbs the dark state $|\psi_0\rangle$. This perturbation will not result in the coupling of $|\psi_0\rangle$ to the bright states $|\psi_\pm\rangle$ as long as the shift β_{ab} is small compared to the exchange interaction strength B, since the latter determines the energy splitting of the bright eigenstates and thereby the width of the dark resonance. Yet, during the gate execution the small but finite population of the energy shifted state $|a_c b_t\rangle$ will result in a phase shift of the dark state, $\phi = \int_0^{T_t} \beta_{ab} P_{Ry}(t)dt$. This phase can be amended, as described in [23] and in Appendix C. Otherwise, we can tune the Förster frequency defect $\delta\omega$ for the transition $|r_c r_t\rangle \to |a_c b_t\rangle$ to exactly compensate this level shift, $\delta\omega = -\beta_{ab}$, as discussed in Appendix B. Then the phase shift ϕ will vanish for any resonant pulse $\Omega_t(t)$.

We have verified the above qualitative results by exact numerical simulations of the dynamics of the two-atom system, as detailed in Appendix B. We use smooth 2π laser pulses $\Omega_t(t)$ applied to the target qubit during step ii and stronger π pulses $\Omega_{c0} = 4\Omega_{t0}$ applied to the control atom in steps i and iii. In Fig. 3 we show the error probabilities $E = 1 - F$ of the phase gate. The gate fidelity F is obtained by averaging over all possible two-qubit input states, as described in Appendix B and [42]. We observe that the error follows approximately the linear scaling $E = \eta/(B\tau)$, but for large values of $B\tau \gtrsim 10^6$ the numerically obtained error probabilities start to deviate from the analytic estimate of the

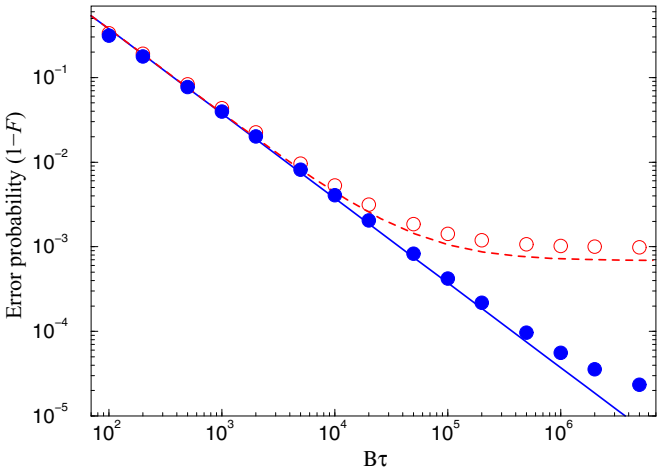

FIG. 3. Error probabilities $E = (1 - F)$ of the phase gate, averaged over all the input states, versus $B\tau$. Filled blue circles correspond to smooth 2π laser pulses $\Omega_t(t)$ applied to the target qubit, while empty red circles correspond to nonadiabatic (square) pulses of the same area and duration. The results are obtained by numerical simulation of the dynamics of the two-atom system with a non-Hermitian Hamiltonian, as described in Appendix B. The solid blue line shows $E = \eta/(B\tau)$ and the dashed red line shows $E = \eta/(B\tau) + \alpha^2/16$. All Rydberg states decay with the same rate Γ, while qubit states $|0\rangle$ and $|1\rangle$ do not decay. We used $\alpha \equiv \Omega_{t0}/B = 0.10472$ ($\eta = 37.5$) resulting in the nonadiabatic transition errors $E_{na} \simeq 2 \times 10^{-6}$ for smooth (shifted Gaussian) pulses.

error during only step ii. This is due the contribution of the additional error $\sim 10^{-5}$ stemming from the decay of the control qubit $E_{decay} \simeq \pi\Gamma/\Omega_{c0}$ during steps i and iii, nonadiabatic transitions and leakage from the dark state E_{na}, and imperfect phase compensation. Nevertheless, we obtain that the average fidelity reaches $F = 0.99995$ for $B\tau \gtrsim 10^6$.

For comparison, we also show in Fig. 3 the results of simulations for the gate performed with square 2π pulses acting on the target qubit. Now, starting from the values of $B\tau \geqslant 10^5$, the error probability significantly deviates from the linear scaling, which is due to the breakdown of adiabaticity leading to the residual Rydberg population of the target atom $\sim\Omega_t^2/16B^2$. There is also sizable population leakage to other Rydberg states not accounted for by the analytic estimate of the gate error. We note that this error is of the same magnitude as the rotation error due to imperfect Rydberg blockade [23]. As we show in Appendix C, this error can also be avoided in the usual Rydberg blockade scenario [16], using either adiabatic pulses to excite and deexcite the target atom, or by applying a square pulse of proper amplitude $\Omega_t = \frac{B_{sh}}{\sqrt{4k^2-1}}$ ($k \in \mathbf{N}$) which accomplishes both a full resonant 2π Rabi cycle and a full precession of the two-level Bloch vector with the generalized off-resonant Rabi frequency $\bar{\Omega} \equiv \sqrt{B_{sh}^2 + \Omega_t^2}$. Such pulses, however, contribute interaction phases to the quantum state amplitudes which can only be compensated for if we know precisely the interatomic distance and thereby the interaction strength B_{sh}. Moreover, during the standard blockade or interaction gates with dispersive interatomic interaction (static dipole-dipole or van der Waals level shift B_{sh}), for any nonvanishing probability of double Rydberg excitation, the atoms are subject to forces due to the spatially dependent potential.

IV. CONCLUSIONS

In summary, we have examined the phase gate performance using strong resonant dipole-dipole interactions between pairs of atoms in Rydberg states. Our gate assumes atomic level and laser excitation schemes which are similar to the ones used in current experiments. Employing adiabatic excitation of the Rydberg states of atoms with smooth laser pulses, we find favorable scaling of the intrinsic gate errors $E \propto (\Gamma/B)$ with the ratio of the Rydberg state decay rate Γ to the interaction strength B, which should be contrasted with the optimized error probability $E \propto (\Gamma/B)^{2/3}$ obtained in the previous studies [21–23] with nonadiabatic pulses. The better scaling of the gate error probability is due to nearly complete elimination of the residual Rydberg excitation of the imperfectly blockaded atom. The corresponding gate fidelity can reach $F > 0.9999$ for $B/\Gamma \simeq 10^6$. The ultimate limit on gate fidelity depends on the value of B/Γ and the ability to suppress other technical sources of errors. While the analysis of Sec. III shows that generically $B\tau \lesssim 10^7$, the precise limit may be higher. Thus, for cases 1–5 in Appendix A, we find that $B\tau$ can be as high as 4×10^7 in a cryogenic environment at 4 K, which implies that a fidelity of $F = 1 - 10^{-5}$ is feasible.

We have focused in this paper on the intrinsic gate error E due to the decay of the Rydberg states and their finite interaction strength. In any real experiment, however, there will also be technical errors, due to, e.g., the laser phase fluctuations and Doppler shifts leading to dephasing γ of the atomic transition, and variations of the laser pulse duration or amplitude leading to pulse area uncertainty $\delta\theta$. If we require that $\gamma \lesssim \Gamma/2$ and $\delta\theta \lesssim \sqrt{E}$, these errors will not exceed the intrinsic error E and adversely affect the system.

ACKNOWLEDGMENTS

This paper was supported by the U.S. ARL-CDQI program through Cooperative Agreement No. W911NF-15-2-0061, the European Union H2020 FET-Proactive project RySQ, and the Villum Foundation.

APPENDIX A: RESONANT DIPOLE-DIPOLE INTERACTIONS OF RYDBERG STATE ATOMS

In the main text, we discuss the realization of a quantum gate using a two-atom dark state resonance which employs a resonant dipole-dipole exchange interaction between a pair of Rydberg atoms in a state $|r_c r_t\rangle$ and a state $|a_c b_t\rangle$ with the same energy, $\varepsilon_{r_c} + \varepsilon_{r_t} = \varepsilon_{a_c} + \varepsilon_{b_t}$ (see Fig. 1). The most obvious choice of Rydberg states that exhibit strong resonant exchange interaction is $|r_c\rangle = |b_t\rangle \equiv ns_{1/2}$ and $|r_t\rangle = |a_c\rangle \equiv np_{3/2}$ with a large principal quantum number $n \sim 100$. State $|1_c\rangle$ of the control atom can then be coupled to the Rydberg state $|r_c\rangle$ by a two-photon transition via a virtual intermediate state involving two optical photons (or a UV and a MW photon). State $|1_t\rangle$ of the target atom can be coupled to the Rydberg state $|r_t\rangle$ by a single UV photon.

While being automatically resonant for the $|r_c r_t\rangle \leftrightarrow |a_c b_t\rangle$ transition, this choice of Rydberg states, however, presents problems associated with near-resonant coupling to other, unwanted states. Recall that, in the absence of external electric or magnetic fields, the energies of the Rydberg states are given by $\varepsilon_{nl} \equiv \hbar\omega_{nl} = -\frac{\mathrm{Ry}}{(n-\delta_l)^2}$, where Ry is the Rydberg constant and δ_l is the quantum defect for the angular momentum states with $l = s, p, \ldots$ [1,36]. For large n, we then obtain that the frequency mismatch $\delta\omega_{rr(ab)} = \omega_{ns} + \omega_{np} - \omega_{(n+dn)p} - \omega_{(n-dn)s}$ for transitions from $|ns,np\rangle$ to unwanted states $|(n+dn)p,(n-dn)s\rangle$ scales as $\delta\omega_{rr} \simeq \delta\omega_{\mathrm{F}}\frac{3(dn+\delta_S-\delta_P)}{n} \ll \delta\omega_{\mathrm{F}}$, rather than the familiar Förster defect $\delta\omega_{\mathrm{F}} = \mathrm{Ry}\frac{2dn}{n^3}$.

1. Stark tuned Förster resonances

We can mitigate this problem by resorting instead to the Stark tuned Förster resonances, which have been demonstrated in [43,44]. In principle, Stark tuning with an appropriate external static electric field E_{St} can render any pair of two-atom states $|r_c r_t\rangle$ and $|a_c b_t\rangle$ degenerate. These two-atom states may still couple to many other states resulting in leakage and gate errors, and our task is to search for state combinations minimizing this leakage. We consider two types of leakage channels, as shown in Fig. 4: forward leakage where $|r_c r_t\rangle$ couples to states $|a'_c b'_t\rangle$ with strength B_{rr} and Förster defect $\delta\omega_{rr}$, and backward leakage that couples $|a_c b_t\rangle$ to states $|b'_c a'_t\rangle$ with strength B_{ab} and Förster defect $\delta\omega_{ab}$. We neglect higher-order leakage processes where the states $|a'_c b'_t\rangle$ and $|b'_c a'_t\rangle$ couple to $|b''_c a''_t\rangle$ and $|a''_c b''_t\rangle$, etc.

We have searched for suitable Cs atom pair Rydberg states by choosing $|r_c r_t\rangle$ and $|a_c b_t\rangle$ and then finding the static Stark field E_{St}, directed along the quantization axis, that makes the pairs energy degenerate. We used standard expressions for the scalar and tensor polarizabilities [45] in the fine-structure basis calculated by summing over all dipole allowed transitions over a range of principal quantum numbers of ± 20 from each state. Small hyperfine corrections have been neglected. Radial matrix elements between Rydberg states were calculated using the quasiclassical (WKB) approximation [46] with quantum defect values taken from [47,48]. The effective matrix elements were not corrected for state mixing due to E_{St}.

We checked all possible dipole allowed transitions from $|r_c r_t\rangle$ and $|a_c b_t\rangle$ to the leakage states with the change of principal quantum number up to ± 5 from the resonant states. The Förster energy defects of leakage state pairs were calculated for E_{St} corresponding to the $|r_c r_t\rangle \leftrightarrow |a_c b_t\rangle$ resonance. The two-atom dipolar coupling coefficient is given

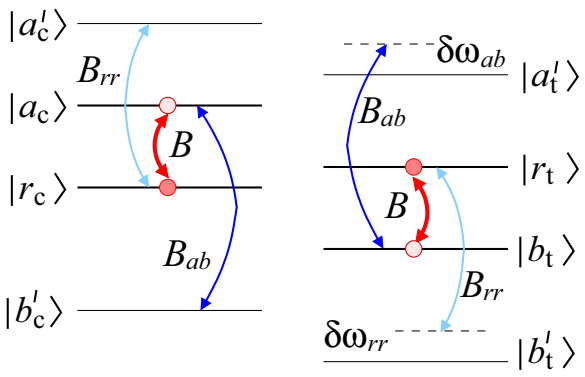

FIG. 4. Energy-level structure of Rydberg states for Stark tuned Förster interaction. Resonant lasers couple the qubit states $|1_{c,t}\rangle$ of the control and target atoms to the corresponding Rydberg states $|r_{c,t}\rangle$ (see Fig. 1). A static electric field shifts the Rydberg states making the two-atom states $|r_c r_t\rangle$ and $|a_c b_t\rangle$ energy degenerate and resonantly coupled via exchange interaction with strength B. The forward leakage channel couples $|r_c r_t\rangle$ to $|a'_c b'_t\rangle$ with strength B_{rr} and energy defect $\delta\omega_{rr}$. The backward leakage channel couples $|a_c b_t\rangle$ to $|b'_c a'_t\rangle$ with strength B_{ab} and energy defect $\delta\omega_{ab}$.

by the general expression

$$C_3 = -\frac{e^2}{4\pi\epsilon_0}\frac{\sqrt{6}(4\pi)^{3/2}}{3\sqrt{5}}\sum_{M,q}(-1)^M C^{2,-M}_{1,q,1,-M-q} \times Y_{2,M}(\hat{\varepsilon})(rY_{1,q})^{(c)}(rY_{1,-M-q})^{(t)}, \quad \text{(A1)}$$

where $C^{\cdots}_{\cdots}$ is a Clebsch-Gordan coefficient, $Y_{2,M}$ is a spherical harmonic, $\hat{\varepsilon}$ is a unit vector pointing from atom (c) to atom (t), and $(rY_{1,q})^{(c)}$ and $(rY_{1,-M-q})^{(t)}$ are the relative electron positions for each atom in spherical coordinates. We evaluate the above expression for $\hat{\varepsilon}$ perpendicular to the quantization axis. This corresponds to the geometry of a planar array of atoms that may be individually addressed while having isotropic interactions in the plane, as in [20]. In this geometry, the selection rules for the dipole-dipole interaction are $\Delta M = 0, \pm 2$. Fewer leakage channels occur with $\hat{\varepsilon}$ along the quantization axis which limits the interactions to $\Delta M = 0$, but such a geometry is less convenient for a multiqubit implementation of quantum information processing with trapped neutral atoms.

In Tables I and II we show several possible choices of the Rydberg atom pair states $|r_c r_t\rangle$ and $|a_c b_t\rangle$. One possibility (cases 1–3) is $|r_c r_t\rangle = |n_c s_{1/2}, m = 1/2; n_t s_{1/2}, m = 1/2\rangle$, with

TABLE I. Resonant Rydberg atom pair states $|r_c r_t\rangle$ and $|a_c b_t\rangle$, specified as $nl_j m$, with the corresponding dipole-dipole interaction coefficient C_3, parameter $B\tau$ at interatomic separation $x = 3\ \mu$m and temperatures 300 and 4 K, and the strength of the tuning Stark field E_{St}.

Case	$\lvert r_c\rangle$	$\lvert r_t\rangle$	$\lvert a_c\rangle$	$\lvert b_t\rangle$	C_3 (GHz μm^3)	$B\tau(\times 10^6)$ 300 K, 4 K	E_{St} (V/m)
1	$109s_{1/2}1/2$	$101s_{1/2}1/2$	$109p_{3/2}3/2$	$101p_{3/2}3/2$	−64.4	6.5, 32.6	15.4
2	$112s_{1/2}1/2$	$101s_{1/2}1/2$	$111p_{3/2}3/2$	$101p_{3/2}3/2$	65.3	6.8, 35.5	5.36
3	$105s_{1/2}1/2$	$94s_{1/2}1/2$	$105p_{3/2}3/2$	$94p_{3/2}3/2$	−51.4	4.7, 23.1	20.1
4	$112p_{3/2}3/2$	$101p_{3/2}3/2$	$112s_{1/2}1/2$	$101s_{1/2}1/2$	−68.2	7.1, 38.5	14.2
5	$95p_{3/2}3/2$	$84p_{3/2}3/2$	$95s_{1/2}1/2$	$84s_{1/2}1/2$	−33.0	2.7, 10.7	34.7

TABLE II. The dominant forward and backward leakage states, corresponding to the largest absolute values of parameters $\beta_{rr} = B_{rr}^2/\delta\omega_{rr}$ and $\beta_{aa} = B_{aa}^2/\delta\omega_{aa}$, for the cases 1–5 in Table I. The last column gives the population missing from state $|r_c 1_t\rangle$ after step ii as found from numerical integration of the Schrödinger equation with Hamiltonian (A2) and the laser parameters given there.

Case	$\lvert a'_c\rangle$	$\lvert b'_t\rangle$	B_{rr}/B	$\delta\omega_{rr}/2\pi$ (MHz)	$\lvert b'_c\rangle$	$\lvert a'_t\rangle$	B_{ab}/B	$\delta\omega_{ab}/2\pi$ (MHz)	$1-P_{\lvert r1\rangle}(T_t)$
1	$109p_{1/2}(-1/2)$	$101p_{3/2}(-1/2)$	−0.49	65	$108d_{5/2}5/2$	$99d_{5/2}5/2$	−0.64	190	1.4×10^{-5}
2	$111p_{1/2}(-1/2)$	$101p_{1/2}(-1/2)$	0.66	−259	$110d_{5/2}5/2$	$100d_{5/2}5/2$	−2.17	1990	1.7×10^{-6}
3	$105p_{1/2}(-1/2)$	$94p_{3/2}(-1/2)$	−0.49	247	$104d_{5/2}5/2$	$92d_{5/2}5/2$	−0.64	−185	5.5×10^{-5}
4	$111d_{5/2}(5/2)$	$99d_{5/2}(5/2)$	−0.64	−75	$112p_{1/2}(-1/2)$	$101p_{3/2}(-1/2)$	−0.49	171	9.5×10^{-6}
5	$94d_{5/2}(5/2)$	$82d_{5/2}(5/2)$	−0.64	−478	$95p_{3/2}3/2$	$84p_{1/2}(-1/2)$	0.28	122	6.4×10^{-6}

the Stark field set for resonance with $|a_c b_t\rangle = |n_c p_{3/2}, m = 3/2; n_t p_{3/2}, m = 3/2\rangle$. The laser excitation of the Rydberg states $|r_c\rangle$ and $|r_t\rangle$ from the Cs ground state requires two-photon transitions. The forward leakage channels from $|r_c r_t\rangle$ are to $p_{1/2}$ or $p_{3/2}$ states. The backward leakage channels couple $|a_c b_t\rangle$ to either two s states with different n, two d states, or an s and a d state. Another possibility (cases 4 and 5) is $|r_c r_t\rangle = |n_c p_{3/2}, m = 3/2; n_t p_{3/2}, m = 3/2\rangle$ tuned to resonance with $|a_c b_t\rangle = |n_c s_{1/2}, m = 1/2; n_t s_{1/2}, m = 1/2\rangle$. The Rydberg states $|r_c\rangle$ and $|r_t\rangle$ can now be reached with one UV photon starting from the Cs ground state. Although the fine-structure splitting between $np_{3/2}$ and $np_{1/2}$ states is small at large n, undesired coupling to $np_{1/2}$ is strongly suppressed in the heavy alkali-metal atoms [49]. Note that state $|a_c b_t\rangle$ can couple strongly with $|n_c p_{1/2}; n_c p_{1/2}\rangle$, but the energy separation of the np fine-structure states is increased in the presence of a Stark field.

2. Numerical estimates of the leakage errors

To estimate the gate error due to the leakage of population of states $|r_c r_t\rangle$ and $|a_c b_t\rangle$ to the nonresonant states $|a'_c b'_t\rangle$ and $|b'_c a'_t\rangle$, we solve the Schrödinger equation for the two-atom system subject to the Hamiltonian

$$H_5/\hbar = H_3/\hbar + \delta\omega_{rr}|b'_t\rangle\langle b'_t| + \delta\omega_{ab}|a'_t\rangle\langle a'_t| + B_{rr}|a'_c b'_t\rangle\langle r_c r_t| + B_{ab}|b'_c a'_t\rangle\langle a_c b_t| + \text{H.c.}, \quad \text{(A2)}$$

where H_3 is the Hamiltonian of Eq. (1). Starting with the initial state $|r_c 1_t\rangle$, we apply a smooth pulse of duration $T_t = 2\pi/\alpha B$ and a (shifted) Gaussian temporal shape $\Omega_t(t) = A[e^{-(t-T_t/2)^2/(2\sigma^2)} - e^{-(T_t/2)^2/(2\sigma^2)}]$, where A is chosen such that $\theta_t = \int_0^{T_t}\Omega_t dt = 2\pi$, and we take $\sigma = T_t/5$ leading to the peak Rabi frequency $\Omega_t(T_t/2) = 2.1\times 2\pi/T_t$. Numerical simulations were performed with $B/2\pi = 350$ MHz, $\alpha = 0.1$, $T_t = 29$ ns, and a peak Rabi frequency of $\Omega_t(T_t/2)/2\pi = 74$ MHz. In Table II, last column, we show the population missing from state $|r_c 1_t\rangle$ at the end of the pulse. In all cases, the population rotation error is in the range of 2×10^{-6}–5×10^{-5}, with the smallest error obtained for case 2. A full analysis including all the leakage channels will undoubtedly show larger errors. The results presented here, however, account for the dominant leakage and we are optimistic that nonadiabatic effects may further be reduced by pulse shaping [24].

APPENDIX B: DETAILS OF THE NUMERICAL CALCULATIONS

In Fig. 3 we present the results of numerical simulations of the complete phase gate between the control and target qubits represented by the atoms. The system we simulate consists of two six-level atoms described by the Hamiltonian of the form

$$H = H_{\text{MW}} + H_{\text{L}} + H_{\text{Ry}}. \quad \text{(B1)}$$

Here the first term describes the qubit states of the atoms, $|0_{c,t}\rangle$ and $|1_{c,t}\rangle$, and their manipulation by the microwave fields,

$$H_{\text{MW}}/\hbar = -\Delta^{(c)}_{\text{MW}}(t)|0_c\rangle\langle 0_c| - \Delta^{(t)}_{\text{MW}}(t)|0_t\rangle\langle 0_t| \times \tfrac{1}{2}\Omega_{\text{MW}}(t)(|1_c\rangle\langle 0_c| + |1_t\rangle\langle 0_t|) + \text{H.c.}, \quad \text{(B2)}$$

where $\Omega_{\text{MW}}(t)$ is the Rabi frequency of the pulsed microwave field seen by both atoms, and the selectivity is provided by setting the detuning $\Delta^{(c,t)}_{\text{MW}}(t)$ of each atom to either $\Delta_{\text{MW}} = 0$ or $\Delta_{\text{MW}} \gg |\Omega_{\text{MW}}|$. This can be done by using nonresonant laser light tightly focused onto the selected atom to induce an ac Stark shift of one of the qubit states [31]. We always start with the two-atom state $|00\rangle$ and prepare one of the four input states $|00\rangle$, $|01\rangle$,$|10\rangle$,$|11\rangle$ by applying a microwave π pulse, with the atom(s) required to switch to state $|1\rangle$ being resonant ($\Delta_{\text{MW}} = 0$), and the atom(s) required to remain in $|0\rangle$ being strongly detuned ($\Delta_{\text{MW}} = 100|\Omega_{\text{MW}}|$). The Hadamard gates on the atoms can also be performed in the same way, with the $\pi/2$ microwave pulse having the phase $\arg(\Omega_{\text{MW}}) = -\pi/2$.

The second term of Eq. (B1) describes the resonant laser coupling of the qubit states $|1_{c,t}\rangle$ of the control and target atoms to the Rydberg states $|r_{c,t}\rangle$:

$$H_{\text{L}}/\hbar = \tfrac{1}{2}\Omega_c(t)|r_c\rangle\langle 1_c| + \tfrac{1}{2}\Omega_t(t)|r_t\rangle\langle 1_t| + \text{H.c.} \quad \text{(B3)}$$

The lasers are focused onto the atoms, and we apply strong π pulses to the control atom in steps i and iii of the protocol, and a smooth 2π pulse to the target atom in step ii. The temporal shape of the target laser pulse is

$$\Omega_t(t) = A[e^{-(t-T_t/2)^2/(2\sigma^2)} - e^{-(T_t/2)^2/(2\sigma^2)}] \quad \text{(B4)}$$

with

$$A = \frac{e^{T_t^2/(8\sigma^2)} - 1}{1 - e^{-(T_t/2)^2/(2\sigma^2)}} \frac{\sqrt{2\pi}}{\sigma e^{T_t^2/(8\sigma^2)}\text{erf}[T_t/(2^{3/2}\sigma)] - T_t}.$$

The pulse duration is $T_t = 2\pi/\Omega_{t0}$ with $\Omega_{t0}/B = \alpha = 0.10472$, and we take $\sigma = T_t/5$. The shifted Gaussian pulses of the form (B4) have the advantage of being smooth, finite-duration pulses that can be readily implemented experimentally. The time intervals between the laser pulses in steps i–iii are set to $T_t/20$.

Finally, the last term of Eq. (B1) describes the Rydberg states of atoms and their interactions:

$$H_{\rm Ry}/\hbar = \delta\omega|b_{\rm t}\rangle\langle b_{\rm t}| + \delta\omega_{rr}|b'_{\rm t}\rangle\langle b'_{\rm t}| + \delta\omega_{ab}|a'_{\rm t}\rangle\langle a'_{\rm t}| + (B|a_{\rm c}b_{\rm t}\rangle\langle r_{\rm c}r_{\rm t}| + B_{rr}|a'_{\rm c}b'_{\rm t}\rangle\langle r_{\rm c}r_{\rm t}| + B_{ab}|b'_{\rm c}a'_{\rm t}\rangle\langle a_{\rm c}b_{\rm t}| + {\rm H.c.}), \quad \text{(B5)}$$

where we include the Förster defect $\delta\omega$ on the Stark tuned transition $|r_{\rm c}r_{\rm t}\rangle \leftrightarrow |a_{\rm c}b_{\rm t}\rangle$. When the transitions to the unwanted states $|a'_{\rm c}b'_{\rm t}\rangle$ and $|b'_{\rm c}a'_{\rm t}\rangle$ are nonresonant, i.e., the corresponding Förster defects are large, $\delta\omega_{rr(ab)} > B_{rr(ab)}$, the leakage from the two-atom dark state is suppressed. Yet, the nonresonant couplings induce second-order level shifts of states $|r_{\rm c}r_{\rm t}\rangle$ and $|a_{\rm c}b_{\rm t}\rangle$, given by $\beta_{rr} = B_{rr}^2/\delta\omega_{rr}$ and $\beta_{ab} = B_{ab}^2/\delta\omega_{rr}$, respectively. The dark state $|\psi_0\rangle$ is insensitive to the small energy shift β_{rr} of the intermediate state $|r_{\rm c}r_{\rm t}\rangle$. But the energy shift β_{ab} of state $|a_{\rm c}b_{\rm t}\rangle$ perturbs the dark resonance. If β_{ab} is small compared to the energy splitting $\pm B$ of the bright eigenstates $|\psi_\pm\rangle$ (see Sec. II), they will not be populated from $|\psi_0\rangle$ under the adiabatic condition. However, during the phase gate sequence starting from state $|r_{\rm c}1_{\rm t}\rangle$, the small but finite population $P_{\rm Ry}(t) = \frac{\Omega_{\rm t}^2(t)}{4B^2+\Omega_{\rm t}^2(t)}$ of state $|a_{\rm c}b_{\rm t}\rangle$ will result in the dark state accumulating the phase $\phi = \int_0^{T_{\rm t}} \beta_{ab} P_{\rm Ry}(t)dt \approx \kappa \frac{\pi^2\beta_{ab}}{B^2 T_{\rm t}}$, where $\kappa = O(1)$ depends on the $\Omega_{\rm t}(t)$ pulse shape. For example, $\kappa = \frac{\pi^2}{8} \simeq 1.23$ for the pulse $\Omega_{\rm t}(t) = \frac{1}{2}\pi\Omega_{\rm t0}\sin(\pi t/T_{\rm t})$, and $\kappa \simeq 1.52$ for the pulse of Eq. (B4) [$\kappa = 1$ for the square, nonadiabatic pulse $\Omega_{\rm t}(t) = \Omega_{\rm t0}$]. In order to suppress the undesired phase shift, we assume that the Förster defect $\delta\omega$ can be tuned to compensate the level shift β_{ab}. In the numerical simulations of Fig. 3 we thus set $\delta\omega = -\beta_{ab}$. There we choose $B_{rr(ab)} = B/2$ and $\delta\omega_{rr(ab)} = 3B_{rr(ab)}$, but other values of $B_{rr(ab)} < \delta\omega_{rr(ab)}$ yield similar results for the gate fidelities under the adiabatic conditions. For the nonadiabatic (square) pulse $\Omega_{\rm t}$, however, we observe significant population leakage to states $|a'_{\rm c}b'_{\rm t}\rangle$ and $|b'_{\rm c}a'_{\rm t}\rangle$, in addition to the nonvanishing residual population of the bright states $|\psi_\pm\rangle$ after the pulse. This explains the slightly larger (by a factor of $\sim$1.4) gate error for $B\tau \gtrsim 10^5$ as compared to the analytic estimates which take into account only the population of the bright states.

In the numerical simulations of Fig. 3, we neglect decay and decoherence of the qubit states $|0_{\rm c,t}\rangle$ and $|1_{\rm c,t}\rangle$ and assume that all the Rydberg states $|\rho_{\rm c,t}\rangle$ ($\rho = r,a,a',b,b'$) of atoms (c) and (t) decay with the same rate $\Gamma = 1/\tau$. This process is described by adding the Lindbladian decay term $\mathcal{L}^2 = \sum_{j={\rm c,t}}\sum_\rho \Gamma|\rho_j\rangle\langle\rho_j|$ to the Hamiltonian of Eq. (B1), making it thus non-Hermitian:

$$\tilde{H} = H - \frac{i}{2}\hbar\mathcal{L}^2. \quad \text{(B6)}$$

We solve the Schrödinger equation $\partial_t|\Psi\rangle = -\frac{i}{\hbar}\tilde{H}|\Psi\rangle$ for the total state vector $|\Psi\rangle$ of the systems of two six-level atoms. The decay of the Rydberg states thus results in the loss of the total population of the system (decreasing the norm $\langle\Psi|\Psi\rangle$ due to population of states outside the basis states). This slightly overestimates the gate error by disregarding processes that may repopulate the qubit states from the Rydberg states by the spontaneous decay.

In calculating the error probabilities for the phase gate, for each two-qubit input state $|\Psi(t_{\rm in})\rangle = |00\rangle,|01\rangle,|10\rangle,|11\rangle$, we propagate the state vector $|\Psi(t)\rangle$ of the system until the end of the sequence ($t = t_{\rm out}$) involving the preparatory microwave and optical pulses as described above. From the four output states $|\Psi(t_{\rm out})\rangle$, we obtain the 4×4 transformation matrix U, and then calculate the average fidelity [42] of the two-qubit gate via $F = [{\rm Tr}(MM^\dagger) + |{\rm Tr}(M)|^2]/(20)$ with $M = U_{\rm CZ}^\dagger U$, where $U_{\rm CZ}$ is the transformation matrix of the ideal phase gate. The average gate error is identified with the infidelity $E = 1 - F$.

APPENDIX C: RYDBERG BLOCKADE GATE

For comparison, we now discuss the relevant properties of the Rydberg blockade gate performed in the conventional way [16] via excitation of (identical) Rydberg states $|r_{\rm c,t}\rangle$ of the control and target atoms.

Strong interatomic interactions can be provided by either static or nonresonant dipole-dipole interaction, which results in the energy shift of double Rydberg excitation, $H_{\rm sh} = \hbar B_{\rm sh}|r_{\rm c}r_{\rm t}\rangle\langle r_{\rm c}r_{\rm t}|$. The static dipole-dipole interaction occurs between the Stark eigenstates of the atoms in a static electric field. Then atoms in such states $|r\rangle$ possess permanent dipole moments $\wp_r \propto n^2$, leading again to $B_{\rm sh} = C_3/x^3$ with $C_3 \propto n^4$. The dipole-dipole exchange interaction B reduces to the van der Waals type of interaction, $B_{\rm sh} = C_6/x^6$, with $C_6 \simeq C_3^2/\delta\omega_{\rm F} \propto n^{11}$, when the Förster defect $\delta\omega_{\rm F} \propto n^{-3}$ between $|r_{\rm c}r_{\rm t}\rangle$ and (the nearest) $|a_{\rm c}b_{\rm t}\rangle$ is large compared to B. More precisely, we have to sum up the second-order level shifts of $|r_{\rm c}r_{\rm t}\rangle$ due to the nonresonant interaction with all the pairs of states $|a_{\rm c}b_{\rm t}\rangle$, $C_6 \propto \sum_{ab}\frac{|\wp_{ar}\wp_{rb}|^2}{\omega_r+\omega_r-\omega_a-\omega_b}$.

We consider again the dynamics of the two-atom system in state $|r_{\rm c}1_{\rm t}\rangle$ during step ii, but under the scenario of dispersive Rydberg-Rydberg interaction leading to large level shift $B_{\rm sh}$ of the double-excited state $|r_{\rm c}r_{\rm t}\rangle$ (see Fig. 5). The laser field with Rabi frequency $\Omega_{\rm t}$ acts on the transition $|1\rangle \to |r\rangle$ of the target atom, which is now shifted out of resonance by the Rydberg-Rydberg interaction $B_{\rm sh}$. The Hamiltonian of the

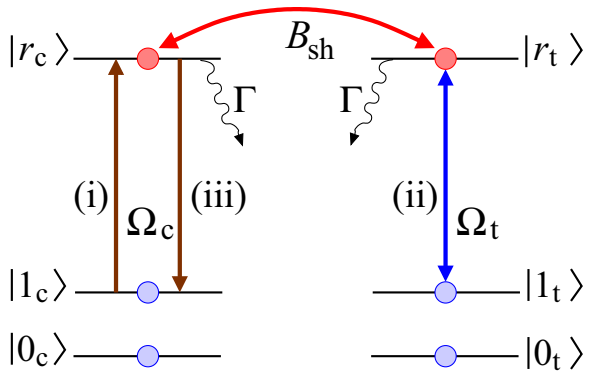

FIG. 5. Schematics of the conventional Rydberg blockade phase gate between the control and target atoms [16]. Atoms in Rydberg states $|r_{\rm c,t}\rangle$ strongly interact with each other via the static or nonresonant dipole-dipole interaction leading to level shift $B_{\rm sh}(\gg\Omega_{\rm t})$ of state $|r_{\rm c}r_{\rm t}\rangle$.

two-level system is then

$$H_2/\hbar = \tfrac{1}{2}(\Omega_t|r_c r_t\rangle\langle r_c 1_t| + \text{H.c.}) + B_{sh}|r_c r_t\rangle\langle r_c r_t|\,. \quad \text{(C1)}$$

The eigenstates of H_2 are $|\psi_\pm\rangle = ([\bar{\Omega} \mp B_{sh}]|r_c 1_t\rangle \pm \Omega_t|r_c r_t\rangle)/\nu_\pm$, with $\bar{\Omega} \equiv \sqrt{B_{sh}^2 + \Omega_t^2}$ and $\nu_\pm^2 = 2(B_{sh}^2 \mp \bar{\Omega}B_{sh} + \Omega_t^2)$, and the corresponding eigenvalues are $\lambda_\pm = \frac{1}{2}(B_{sh} \pm \bar{\Omega})$.

1. Adiabatic driving

For a smooth 2π pulse $\Omega_t(t)$, the initial state $|r_c 1_t\rangle$ is adiabatically connected to the $|\psi_-\rangle$ eigenstate with eigenvalue λ_-, and nonadiabatic transition to $|\psi_+\rangle$ is suppressed for $\Omega_{t0} \ll B_{ex}$. During the pulse, the population of the double-excited Rydberg state $|r_c r_t\rangle$ is $P_{Ry} \simeq \frac{\Omega_t^2}{4B_{ex}^2}$, which returns back to $|r_c 1_t\rangle$ at the end of the pulse, $\Omega_t(t = T_t) \to 0$.

The situation is thus similar to that of the resonant exchange interaction studied in the main text, but there are also important differences. Since the adiabatically connected eigenstate $|\psi_-\rangle$ has nonzero energy $\lambda_-(t) \simeq -\frac{\Omega_t^2(t)}{4B_{sh}}$, at the end of the $\Omega_t(t)$ pulse, state $|r_c 1_t\rangle$ acquires the phase $\phi = \int_0^{T_t} \lambda_-(t)dt$. If both Ω_t and B_{sh} are well defined, this phase is known and can be amended, as described in [23]. [In the present context, correcting the phase shift ϕ involves splitting during step ii the 2π pulse $\Omega_t(t)$ into two smooth π pulses $\Omega_t^{(1)}(t)$ and $e^{i\phi}\Omega_t^{(2)}(t)$ with the relative phase difference ϕ and then, after step iii, applying to the target qubit the operation $\hat{Z}_t = |0_t\rangle\langle 0_t| + e^{-i\phi}|1_t\rangle\langle 1_t|$.] But if there is an uncertainty in the interaction strength, $B_{sh} \to B_{sh} + \delta B$ with $\delta B \simeq \partial_x B_{sh}|_{x=x_0}\delta x$, due to uncertainty δx in the interatomic distance x_0, it will cause phase errors of the target qubit, $\delta\phi \simeq \pi\Omega_t\delta B/B_{sh}^2$. Furthermore, during the pulse Ω_t the pair of atoms in state $|\psi_-\rangle$ occupies the double Rydberg excitation state $|r_c r_t\rangle$ with a finite probability P_{Ry} and, hence, experiences a mechanical force $F = -\hbar\partial_x\lambda_-|_{x=x_0}$, where the x dependence of λ_- stems from B_{sh}.

2. Square pulse of specific amplitude

Perhaps surprisingly, the rotation errors can in principle be avoided even when using nonadiabatic square 2π pulses Ω_t on the target atom, as was studied in detail in [50]. The time-dependent state of the two-level system described by Hamiltonian (C1) can be written as $|\psi(t)\rangle = c_1(t)|r_c 1_t\rangle + c_r(t)|r_c r_t\rangle$, with $c_1(0) = 1$ and $c_r(0) = 0$ corresponding to $|\psi(0)\rangle = |r_c 1_t\rangle$. Neglecting the decay $\Gamma \ll \Omega_t$, the general solution for the amplitudes of state vector $|\psi(t)\rangle$ is given by [34]

$$c_1(t) = e^{i\phi(t)}\left[\cos(\tfrac{1}{2}\bar{\Omega}t) - i\frac{B_{sh}}{\bar{\Omega}}\sin(\tfrac{1}{2}\bar{\Omega}t)\right], \quad \text{(C2a)}$$

$$c_r(t) = e^{-i\phi(t)-\phi_t}\frac{\Omega_t}{\bar{\Omega}}\sin(\tfrac{1}{2}\bar{\Omega}t), \quad \text{(C2b)}$$

where $\phi(t) \equiv \frac{1}{2}B_{sh}t$ and ϕ_t is the laser phase. Our goal is that $c_r(t = T_t) = 0$ at time $T_t = 2\pi/\Omega_t$ of the resonant 2π pulse. We thus require that $\frac{1}{2}\bar{\Omega}T_t = 2\pi k$ ($k \in \mathbf{N}$). We obtain $\Omega_t = \frac{B_{sh}}{\sqrt{4k^2-1}}$, which is largest for $k = 1$: $\Omega_t = \frac{1}{\sqrt{3}}B_{sh}$. The final phase of state $|r_c 1_t\rangle$ would then be $\phi = \sqrt{3}\pi$, which should be amended as described above. Notice, however, that if there are pulse timing or amplitude errors and/or uncertainty in B_{sh}, the averaged (over a small time interval $\Delta t \simeq \pi/\bar{\Omega}$) residual Rydberg population of the target atom will be $P_{Ry} \simeq \frac{\Omega_t^2}{2B_{sh}^2}$. Hence, this method is even less robust with respect to uncertainties of parameters than the above adiabatic methods.

TABLE III. Error probabilities during step ii of the Rydberg-blockade gate, for four two-qubit input states.

Input state	Decay error[a]	Rotation error[b]	Phase error
$\|0_c 0_t\rangle$	0	0	0
$\|0_c 1_t\rangle$	$\frac{\pi\Gamma}{\Omega_t}$	0	0
$\|1_c 0_t\rangle$	$\frac{2\pi\Gamma}{\Omega_t}$	0	0
$\|1_c 1_t\rangle$	$\frac{2\pi\Gamma}{\Omega_t} + \frac{\pi\Gamma\Omega_t}{4B^2}$	$\frac{\Omega_t^2}{2B^2}$	$\frac{\pi\delta B\Omega_t}{B^2}$

[a]For the control and/or target qubit in state $|1\rangle$.
[b]Only for nonadiabatic (square) pulse Ω_t.

3. Gate error estimates

Let us summarize the above results. In Table III we show the error probabilities during step ii of the blockade gate, for the four two-qubit input states. For the gate performed with a smooth (adiabatic) pulse Ω_t, and assuming compensation of the interaction phase ϕ, the error averaged over all the inputs is again $E \simeq \frac{\pi\Gamma}{4}[\frac{5}{\Omega_t} + \frac{\Omega_t}{4B^2}]$, as in the main text for the dark resonance gate. Choosing $\Omega_t = \alpha B$ with $\alpha \ll 1$, we obtain $E \simeq \eta\frac{\Gamma}{B}$ with $\eta \simeq \frac{5\pi}{4\alpha}$. If we also include the phase error of the gate due to uncertainty in the dispersive Rydberg-Rydberg interaction strength, this coefficient would increase accordingly, $\eta \simeq \frac{5\pi}{4\alpha} + \frac{\pi\alpha}{4}\frac{\delta B}{\Gamma}$.

[1] M. Saffman, T. G. Walker, and K. Mølmer, Rev. Mod. Phys. **82**, 2313 (2010).
[2] M. D. Lukin, M. Fleischhauer, R. Côté, L. M. Duan, D. Jaksch, J. I. Cirac, and P. Zoller, Phys. Rev. Lett. **87**, 037901 (2001).
[3] D. Comparat and P. Pillet, J. Opt. Soc. Am. B **27**, A208 (2010).
[4] M. Gärttner, K. P. Heeg, T. Gasenzer, and J. Evers, Phys. Rev. A **88**, 043410 (2013).
[5] I. Lesanovsky and J. P. Garrahan, Phys. Rev. A **90**, 011603(R) (2014).
[6] H. Schempp, G. Günter, M. Robert-de-Saint-Vincent, C. S. Hofmann, D. Breyel, A. Komnik, D. W. Schönleber, M. Gärttner, J. Evers, S. Whitlock, and M. Weidemüller, Phys. Rev. Lett. **112**, 013002 (2014).
[7] N. Malossi, M. M. Valado, S. Scotto, P. Huillery, P. Pillet, D. Ciampini, E. Arimondo, and O. Morsch, Phys. Rev. Lett. **113**, 023006 (2014).
[8] A. Urvoy, F. Ripka, I. Lesanovsky, D. Booth, J. P. Shaffer, T. Pfau, and R. Löw, Phys. Rev. Lett. **114**, 203002 (2015).

[9] I. Bouchoule and K. Mølmer, Phys. Rev. A **65**, 041803(R) (2002).
[10] J. E. Johnson and S. L. Rolston, Phys. Rev. A **82**, 033412 (2010).
[11] N. Henkel, R. Nath, and T. Pohl, Phys. Rev. Lett. **104**, 195302 (2010).
[12] G. Pupillo, A. Micheli, M. Boninsegni, I. Lesanovsky, and P. Zoller, Phys. Rev. Lett. **104**, 223002 (2010).
[13] J. Zeiher, R. van Bijnen, P. Schauß, S. Hild, J.-Y. Choi, T. Pohl, I. Bloch, and C. Gross, Nat. Phys. **12**, 1095 (2016).
[14] L. F. Buchmann, K. Mølmer, and D. Petrosyan, Phys. Rev. A **95**, 013403 (2017).
[15] J. Zeiher, J.-Y. Choi, A. Rubio-Abadal, T. Pohl, R. van Bijnen, I. Bloch, and C. Gross, arXiv:1705.08372.
[16] D. Jaksch, J. I. Cirac, P. Zoller, S. L. Rolston, R. Cote, and M. D. Lukin, Phys. Rev. Lett. **85**, 2208 (2000).
[17] E. Urban, T. A. Johnson, T. Henage, L. Isenhower, D. D. Yavuz, T. G. Walker, and M. Saffman, Nat. Phys. **5**, 110 (2009); L. Isenhower, E. Urban, X. L. Zhang, A. T. Gill, T. Henage, T. A. Johnson, T. G. Walker, and M. Saffman, Phys. Rev. Lett. **104**, 010503 (2010).
[18] A. Gaëtan, Y. Miroshnychenko, T. Wilk, A. Chotia, M. Viteau, D. Comparat, P. Pillet, A. Browaeys, and P. Grangier, Nat. Phys. **5**, 115 (2009); T. Wilk, A. Gaëtan, C. Evellin, J. Wolters, Y. Miroshnychenko, P. Grangier, and A. Browaeys, Phys. Rev. Lett. **104**, 010502 (2010).
[19] L. Beguin, A. Vernier, R. Chicireanu, T. Lahaye, and A. Browaeys, Phys. Rev. Lett. **110**, 263201 (2013).
[20] K. M. Maller, M. T. Lichtman, T. Xia, Y. Sun, M. J. Piotrowicz, A. W. Carr, L. Isenhower, and M. Saffman, Phys. Rev. A **92**, 022336 (2015).
[21] M. Saffman and T. G. Walker, Phys. Rev. A **72**, 022347 (2005).
[22] L. Isenhower, M. Saffman, and K. Mølmer, Quant. Info. Proc. **10**, 755 (2011).
[23] X. L. Zhang, A. T. Gill, L. Isenhower, T. G. Walker, and M. Saffman, Phys. Rev. A **85**, 042310 (2012).
[24] L. S. Theis, F. Motzoi, F. K. Wilhelm, and M. Saffman, Phys. Rev. A **94**, 032306 (2016).
[25] K. M. Svore, D. P. DiVincenzo, and B. M. Terhal, Quantum Inf. Comput. **7**, 297 (2007).
[26] F. M. Spedalieri and V. P. Roychowdhury, Quantum Inf. Comput. **9**, 0666 (2009).
[27] C.-Y. Lai, G. Paz, M. Suchara, and T. A. Brun, Quantum Inf. Comput. **14**, 0807 (2014).
[28] W. Li, C. Ates, and I. Lesanovsky, Phys. Rev. Lett. **110**, 213005 (2013).
[29] D. Petrosyan and K. Mølmer, Phys. Rev. Lett. **113**, 123003 (2014).
[30] D. D. Bhaktavatsala Rao and K. Mølmer, Phys. Rev. A **89**, 030301(R) (2014).
[31] T. Xia, M. Lichtman, K. Maller, A. W. Carr, M. J. Piotrowicz, L. Isenhower, and M. Saffman, Phys. Rev. Lett. **114**, 100503 (2015).
[32] M. Saffman, J. Phys. B **49**, 202001 (2016).
[33] M. Nielsen and I. Chuang, *Quantum Computation and Quantum Information* (Cambridge University, Cambridge, England, 2000).
[34] P. Lambropoulos and D. Petrosyan, *Fundamentals of Quantum Optics and Quantum Information* (Springer, Berlin, 2007).
[35] K. Bergmann, H. Theuer, and B. W. Shore, Rev. Mod. Phys. **70**, 1003 (1998).
[36] T. F. Gallagher, *Rydberg Atoms* (Cambridge University, Cambridge, England, 1994).
[37] F. Gounand, J. de Physique **40**, 457 (1979).
[38] I. I. Beterov, I. I. Ryabtsev, D. B. Tretyakov, and V. M. Entin, Phys. Rev. A **79**, 052504 (2009); **80**, 059902(E) (2009).
[39] J. H. Wesenberg, K. Mølmer, L. Rippe, and S. Kröll, Phys. Rev. A **75**, 012304 (2007).
[40] E. Torrontegui, S. Ibanez, S. Martinez-Garaot, M. Modugno, A. del Campo, D. Guery-Odelin, A. Ruschhaupt, Xi Chen, and J. G. Muga, Adv. At. Mol. Opt. Phys. **62**, 117 (2013).
[41] F. Motzoi, J. M. Gambetta, P. Rebentrost, and F. K. Wilhelm, Phys. Rev. Lett. **103**, 110501 (2009); F. Motzoi and F. K. Wilhelm, Phys. Rev. A **88**, 062318 (2013).
[42] L. H. Pedersen, N. M. Møller, and K. Mølmer, Phys. Lett. A **367**, 47 (2007).
[43] I. I. Ryabtsev, D. B. Tretyakov, I. I. Beterov, and V. M. Entin, Phys. Rev. Lett. **104**, 073003 (2010).
[44] S. Ravets, H. Labuhn, D. Barredo, L. Beguin, T. Lahaye, and A. Browaeys, Nat. Phys. **10**, 914 (2014).
[45] F. Le Kien, P. Schneeweiss, and A. Rauschenbeutel, Eur. Phys. J. D **67**, 1 (2013).
[46] B. Kaulakys, J. Phys. B **28**, 4963 (1995).
[47] C.-J. Lorenzen and K. Niemax, Z. Phys. A **315**, 127 (1984).
[48] K.-H. Weber and C. J. Sansonetti, Phys. Rev. A **35**, 4650 (1987).
[49] E. Fermi, Z. Phys. **59**, 680 (1930).
[50] X.-F. Shi, Phys. Rev. Applied **7**, 064017 (2017).